Measurement of the Top-Quark Production Cross Section and Charge Asymmetry at LHCb

R. Aaij *et al.*[*]
(LHCb Collaboration)

(Received 15 December 2025; revised 11 February 2026; accepted 20 April 2026; published 1 June 2026)

The first measurements of the top- and antitop-quark differential production cross sections and the top-quark charge asymmetry in the forward region are presented, using proton-proton collision data collected by the LHCb experiment at a center-of-mass energy of 13 TeV corresponding to an integrated luminosity of 5.4 fb^{-1}. The total production cross sections of top and antitop quarks are also determined. Measurements are performed using the $\mu + b$-jet final state within a fiducial region defined by b-jet $p_{\text{T,jet}} > 50$ GeV and pseudorapidity $2.2 < \eta_{\text{jet}} < 4.0$, with the muon from the W-boson decay required to have $p_{\text{T},\mu} > 25$ GeV and $2.0 < \eta_\mu < 4.5$. The muon and b-jet system must satisfy $p_{\text{T}}(\mu + \text{jet}) > 20$ GeV. The measured integrated production cross sections for the top and antitop quarks are $\sigma_t = 0.95 \pm 0.04 \pm 0.08 \pm 0.02$ pb, $\sigma_{\bar{t}} = 0.81 \pm 0.03 \pm 0.07 \pm 0.02$ pb, where the first uncertainty is statistical, the second systematic, and the third accounts for the luminosity uncertainty. The top-quark charge asymmetry is measured to be $A_C^t = 0.08 \pm 0.03 \pm 0.01$, where the first uncertainty is statistical and the second is systematic. These results are consistent with next-to-leading order Standard Model predictions.

DOI: 10.1103/c1x7-f9wn

In the Standard Model (SM), the top quark (t) is the most massive fundamental particle [1]. Owing to its large Yukawa coupling, it plays a central role in electroweak symmetry breaking and in interactions of the Higgs boson. Moreover, the top quark provides a sensitive probe of physics beyond the SM, including scenarios with modified Higgs couplings or new heavy states [2–4]. At the Large Hadron Collider (LHC), top quarks are mainly produced in pairs with their antiquarks ($t\bar{t}$) via the strong interaction, with a smaller contribution from single-top processes mediated by the electroweak interaction [1]. In the forward region, the SM predicts that about 80% of $t \to Wb$ decays originate from $t\bar{t}$ production, with the remaining 20% dominated by t-channel single-top production [5–7]. The top-quark production cross section is particularly sensitive to the gluon parton distribution function (PDF), especially in the high-Bjorken-x region where current constraints remain weak [8–10]. With its unique forward acceptance, the LHCb detector can probe kinematic regimes inaccessible to the ATLAS and CMS experiments, providing complementary measurements. In particular, forward top production has been suggested as a probe to constrain the gluon PDF at high x at the level of 20% [4].

Within the SM, $t\bar{t}$ production is intrinsically charge symmetric at leading order, and the $gg \to t\bar{t}$ contribution is charge symmetric to all orders. However, next-to-leading-order (NLO) quantum chromodynamics (QCD) effects, driven by quark-antiquark annihilation, induce a small asymmetry. These effects arise from interference between initial- and final-state radiation, as well as between the Born and box diagrams [11]. Although single-top production has a small cross section, its intrinsic asymmetry is enhanced in proton-proton (pp) collisions, where the larger u-quark parton density relative to d-quark parton density leads to a net positive charge asymmetry; the single-top process itself yields a charge asymmetry at the level of about 40% [6,7]. The charge-asymmetry observable is defined as

$$A_C^t = \left(\frac{\sigma_t - \sigma_{\bar{t}}}{\sigma_t + \sigma_{\bar{t}}}\right)_{\eta_\mu}, \tag{1}$$

where σ_t and $\sigma_{\bar{t}}$, respectively, represent the production cross sections of t and $\bar{t}$ quarks in bins of muon pseudorapidity, η_μ, measured in the LHCb laboratory frame. At the LHC, where gluon fusion dominates, the charge asymmetry in $t\bar{t}$ production is significantly diluted. Nevertheless, in the forward region accessible to LHCb, this dilution is reduced, enhancing sensitivity to the charge asymmetry [4]. Theoretical predictions suggest that LHCb may provide the first significant observation of the top-quark charge asymmetry at the LHC [2,4].

The $t\bar{t}$ and single-top production cross sections have been extensively measured by the ATLAS and CMS

[*]Full author list given at the end of the Letter.

Published by the American Physical Society under the terms of the Creative Commons Attribution 4.0 International license. Further distribution of this work must maintain attribution to the author(s) and the published article's title, journal citation, and DOI. Funded by SCOAP[3].

 © 2026 CERN, for the LHCb Collaboration

collaborations at center-of-mass energies of $\sqrt{s} = 5.02$, 7, 8, 13, and 13.6 TeV [12–37]. At LHCb, previous studies have so far been limited to total cross-section measurements at 7, 8, and 13 TeV [38–40]. Measurements of A_C^t were first performed at the Tevatron by the CDF and D0 experiments [41–43], where initial tensions with theoretical predictions were later reduced by improved calculations and updated measurements [44–47]. At the LHC, results from ATLAS [48–53] and CMS [54–58] collaborations have achieved increasing precision. While the most recent ATLAS measurement [53] reports a 4.7σ deviation from zero, the extracted asymmetry remains numerically small and consistent with the SM.

This Letter presents the first measurements of the differential production cross sections of the t and $\bar{t}$ quarks as a function of the muon pseudorapidity in the forward region, the corresponding A_C^t observable, and the integrated production cross sections. The measurement is performed in the $t \to W^+(\to \mu^+\nu_\mu)b$ decay channel [59], using pp collision data collected with the LHCb detector at $\sqrt{s} = 13$ TeV, corresponding to an integrated luminosity of 5.4 fb^{-1}. The measurement is performed in the fiducial phase space defined by the presence of a muon with transverse momentum (defined with respect to the beam axis) $p_{\mathrm{T},\mu} > 25$ GeV in the pseudorapidity range $2.0 < \eta_\mu < 4.5$. [60] Jets are reconstructed using the anti-k_{T} algorithm [61] with radius parameter $R = 0.5$, and are required to satisfy $p_{\mathrm{T,jet}} > 50$ GeV and $2.2 < \eta_{\mathrm{jet}} < 4.0$. The inputs to the jet-clustering algorithm are charged and neutral particles, which are obtained by combining information from all detector subsystems through a particle-flow approach [62].

The top charge asymmetry, A_C^t, is measured via Eq. (1), while the differential cross section for each charge of the final-state muon and each bin in η_μ is determined as

$$\frac{d\sigma_t}{d\eta_\mu} = \frac{(N - N_{\mathrm{bkg}}) \cdot \mathcal{A} \cdot P}{\Delta\eta_\mu \cdot \mathcal{L} \cdot \varepsilon_{\mathrm{sel}} \cdot \varepsilon_{\mathrm{rec}} \cdot \varepsilon_{\mathrm{btag}} \cdot \epsilon_{\mathrm{true}}}, \tag{2}$$

where N is the total number of selected candidates, N_{bkg} is the estimated background contribution, and $\Delta\eta_\mu$ is the width of the bin in η_μ. The integrated luminosity is denoted by $\mathcal{L}$, and the reconstruction, selection, and b-tagging efficiencies are represented by $\varepsilon_{\mathrm{rec}}$, $\varepsilon_{\mathrm{sel}}$, and $\varepsilon_{\mathrm{btag}}$, respectively. The acceptance factor, $\mathcal{A}$, accounts for migrations into and out of the fiducial region, including non-negligible contributions from the $t \to W^+(\to \tau^+\nu_\tau)b$ decay mode. The jet reconstruction purity, P, is defined as the fraction of reconstructed jets within the fiducial region that originate from truth-level jets also contained in the same region. The term ϵ_{true} denotes the truth-level jet reconstruction efficiency, defined as the fraction of truth-level jets within the fiducial region that are successfully reconstructed in the same region.

The LHCb detector [63,64] is a single-arm forward spectrometer covering $2 < \eta < 5$, designed for the study of particles containing b or c quarks. The detector used to collect data for this analysis includes a high-precision tracking system consisting of a silicon-strip vertex detector surrounding the pp interaction region [65], a large-area silicon-strip detector located upstream of a dipole magnet with a bending power of about 4 T m, and three stations of silicon-strip detectors and straw drift tubes [66] placed downstream of the magnet. The tracking system provides a measurement of the momentum, p, of charged particles with a relative uncertainty that varies from 0.5% at low momentum to 1.0% at 200 GeV. The minimum distance of a track to a primary pp collision vertex, the impact parameter (IP), is measured with a resolution of $(15 + 29/p_{\mathrm{T}})$ μm, where p_{T} is measured in GeV. Different types of charged hadrons are distinguished using information from two ring-imaging Cherenkov detectors [67]. Photons, electrons, and hadrons are identified by a calorimeter system consisting of scintillating-pad and preshower detectors, an electromagnetic and a hadronic calorimeter. Muons are identified by a system composed of alternating layers of iron and multiwire proportional chambers [68]. Approximately half of the data were collected with the magnet in each of the two polarity configurations. The online event selection is performed by a trigger system [69,70]. This analysis uses events selected by trigger algorithms that require at least one identified muon with high p_{T}.

Simulation samples are generated using Pythia [71] with a specific LHCb configuration [72]. Final-state radiation is simulated with Photos [73]. The interaction of the generated particles with the detector, and its response, are modeled using the Geant4 toolkit [74] as described in Ref. [75]. Auxiliary signal samples without detector simulation are produced using the Powheg-BOX framework [76–78] at NLO, and interfaced with Pythia for parton showering and hadronization. Alternative NLO predictions produced with the MadGraph [79] framework are employed for cross-checks.

Candidate $t \to W^+(\to \mu^+\nu_\mu)b$ decays are formed from a well-separated muon-jet pair with $\Delta R(\mu, \mathrm{jet}) > 0.5$, where $\Delta R \equiv \sqrt{(\Delta\eta)^2 + (\Delta\phi)^2}$, and $\Delta\eta$ ($\Delta\phi$) is the difference in pseudorapidity (azimuthal angle) between the muon and the jet axis. To suppress semileptonic heavy-flavor backgrounds, the muon IP is required to be less than 0.04 mm [80]. Hadrons misidentified as muons are suppressed by requiring the energy deposit in the electromagnetic (E_{ECAL}) and hadronic (E_{HCAL}) calorimeters to be small, $(E_{\mathrm{ECAL}} + E_{\mathrm{HCAL}})/p < 4\%$, where p is the muon momentum. The relative momentum uncertainty of the muon track, σ_p/p, is required to be less than 10%. Events containing a second, oppositely charged, high-p_{T} muon with $M(\mu^+\mu^-) > 40$ GeV are rejected to suppress $Z/\gamma^*(\to \mu^+\mu^-) + \mathrm{jet}$ contamination.

The jet flavor is identified using a dedicated deep neural network (DNN) classifier, inspired by the DeepJet algorithm [81], and trained using simulated b-, c-, and light-flavor jet samples [82]. The network uses more than 400 input features related to jet properties, including those associated with charged and neutral jet constituents, secondary vertex variables, and global features. The classifier's outputs are three probabilities, P_b, P_c, and P_q, which sum to unity and represent the likelihood of a jet originating from a b-, c-, or light-flavor parton, respectively. To suppress contamination from c jets and light-flavor jets while maximizing the b-jet signal significance, the optimal selection thresholds on the DNN outputs are determined by maximizing the expected signal significance, $S = N_{\text{sim}}/\sqrt{N_{\text{data}}}$, where N_{sim} and N_{data} denote the expected number of simulated top signal and data candidates passing the selection, respectively. The simulated yields are normalized using the theoretical predictions for the production cross section and integrated luminosity. The working point is chosen as $P_b > 0.65$ and $P_q < 0.05$. Despite the tight P_b requirement, residual contamination from misidentified c jets and light-flavor jets remains. To account for this, a template fit to the P_b distribution in data is performed to extract the b-jet fraction, using simulated templates for each jet flavor. The fit yields a b-jet purity of approximately 74%, which is applied as a bin-by-bin weight in η_μ to remove the contributions from c jets and light-flavor jets.

One of the dominant background contributions in this analysis arises from QCD multijet production, particularly from heavy-flavor decays or in-flight hadron decays producing high-p_{T} muons. In signal events such as $t \to W^+(\to \mu^+\nu_\mu)b$, the undetected neutrino carries a significant fraction of the W-boson p_{T}, resulting in a strong momentum imbalance between the muon and the accompanying jet. In contrast, QCD events usually have the muon produced inside or near a jet, leading to a more balanced configuration where the muon and jet p_{T} are similar and the muon is less isolated. To suppress this background, candidates are required to satisfy two further kinematic criteria. First, the p_{T} of the $\mu + b$-jet system, $p_{\text{T,total}} = p_{\text{T}}(j + j_\mu)$, must be greater than 20 GeV, where j denotes the reconstructed jet and j_μ denotes the jet that contains the muon. Second, the muon isolation, defined as $I_\mu = p_{\text{T},\mu}/p_{\text{T},j_\mu}$, must exceed 0.9. The residual QCD background is estimated using a data-driven ABCD method [83] in the ($p_{\text{T,total}}$, I_μ) plane. In this analysis, the ABCD regions are defined as: region A with $p_{\text{T,total}} < 15$ GeV and $I_\mu < 0.9$; region B with $p_{\text{T,total}} < 15$ GeV and $I_\mu > 0.9$; region C with $p_{\text{T,total}} > 20$ GeV and $I_\mu < 0.9$; and region D (the signal region) with $p_{\text{T,total}} > 20$ GeV and $I_\mu > 0.9$, containing 2278 $\mu^+ + b$-jet and 1799 $\mu^- + b$-jet events. The estimated signal yield in region D, N_D^{sig}, is calculated using the generalized ABCD relation.

TABLE I. Relative systematic uncertainties in the t and $\bar{t}$ total cross-section measurements, in percent. The total uncertainties are obtained by summing in quadrature the statistical, total systematic, and luminosity components.

Source	$\Delta\sigma_t/\sigma_t$ (%)	$\Delta\sigma_{\bar{t}}/\sigma_{\bar{t}}$ (%)
b-jet tagging	6.5	6.2
Jet energy scale and resolution	5.0	5.0
ABCD method	2.0	2.1
$Z + b$-jet background	0.2	0.2
$W + b$-jet background	0.9	1.3
Selection efficiency	0.2	0.2
Muon reconstruction efficiency	0.2	0.2
Jet reconstruction efficiency	0.3	0.3
Total systematic (excl. lumi.)	8.5	8.3
Luminosity	2.0	2.0
Statistical	3.8	4.0
Total	9.5	9.4

Electroweak backgrounds are also considered. The $Z + b$-jet background contribution is estimated using $Z(\to \mu^+\mu^-) + b$-jet data candidates together with an acceptance correction factor, taken from the ratio of yields in simulation. Here, the $Z(\to \mu^+\mu^-) + b$-jet category corresponds to partially reconstructed $Z(\to \mu^+\mu^-) + b$-jet decays where one muon falls outside the geometrical acceptance of the LHCb detector. This correction is applied in bins of η_μ and separately for each muon charge. After subtracting the QCD and $Z +$ jet backgrounds, the yield of the remaining $W + b$-jet background contribution is estimated. The relative normalization between $W + b$-jet and $W +$ jet events is taken from the Powheg prediction and cross-checked with MadGraph, with corrections for the b-tagging efficiency applied to match the observed yields.

After background subtraction, the observed signal yields of 1458 (t) and 1231 ($\bar{t}$) are corrected for detector and selection effects. These include the muon reconstruction efficiency, the efficiency of the muon selection criteria, the jet reconstruction efficiency, the b-tagging efficiency and mistag rates, possible bin-to-bin migrations due to the detector resolution, and finally the acceptance difference between the fiducial and signal definitions and a small contamination from W bosons that decay via a τ lepton subsequently producing a muon. The muon reconstruction efficiency, encompassing track reconstruction, identification, and trigger requirements, is estimated with a tag-and-probe method using $Z \to \mu^+\mu^-$ data, following the procedures used in published W- and Z-boson cross-section measurements at LHCb [84–87]. The muon reconstruction efficiency varies across the muon pseudorapidity region, ranging from 64% to 77%. The selection efficiencies are evaluated using simulated $t\bar{t}$ and single-top samples, and vary across the muon pseudorapidity region, ranging from 68% to 75%. The jet reconstruction efficiency is determined from simulated $Z(\to \mu^+\mu^-) +$ jet samples, and is

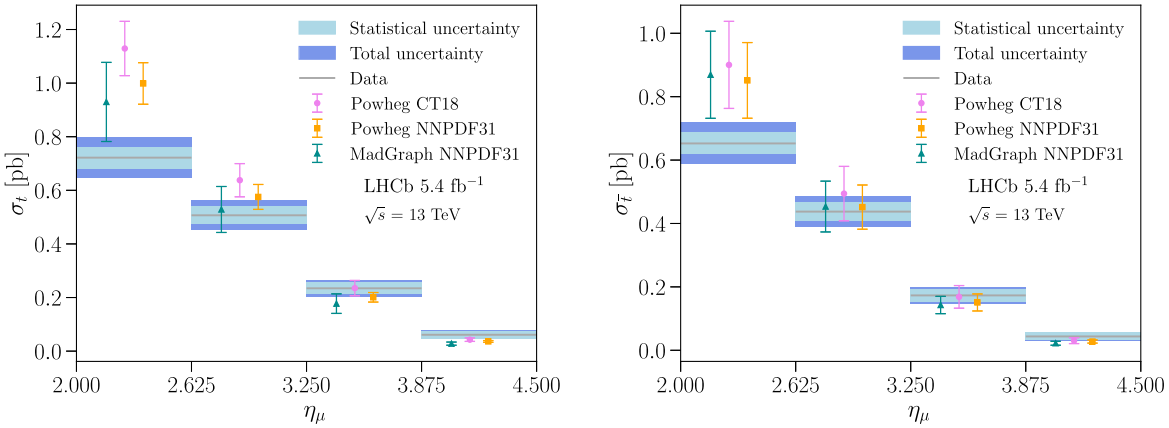


FIG. 1. Differential cross sections for the (left) t and (right) $\bar{t}$ production as a function of the muon pseudorapidity compared with theoretical predictions at NLO.

found to be about 96%. The b-tagging efficiency, based on DNN discriminators, is evaluated using simulated $t\bar{t}$ and single-top samples, and corrected with a data-driven tag-and-probe method in a dijet sample enriched in b jets. The number of b jets before applying the DNN requirement is determined from a fit to the P_b template distribution. After the DNN selection, the mistag fraction, arising from c and light-flavor jets, is subtracted to obtain the final b-jets yield. The mistag probability is evaluated as the fraction of simulated c jets and light-flavor jets passing the same DNN selection under the same tag-and-probe conditions [82]. After applying weights based on the ratio of data to simulation, found to vary between 0.94 and 1.04, the resulting b-tagging efficiency is approximately 56%.

To account for detector-resolution effects, migration corrections for events with a reconstructed jet inside the fiducial region while the truth-level jet is outside, or vice versa, are evaluated with simulations. The corrections from these effects are below 1%. Bin-to-bin migrations in η_μ are found to be negligible, owing to the excellent resolution.

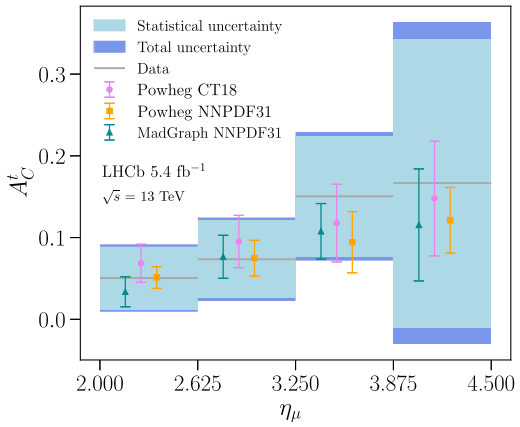


FIG. 2. Measured t-quark charge asymmetry as a function of the muon pseudorapidity compared with theoretical predictions at NLO.

Beyond detector-resolution effects, differences between the definitions of the fiducial region and of the signal region D (in the ABCD method) are taken into account. In the fiducial region, the p_{T} requirement is applied to the vector sum of the muon and the b jet, while in the signal region it is applied to the muon-containing jet combined with the b jet. This mismatch is corrected by using an acceptance factor defined as $\mathcal{A}_{j_\mu} = [N(p_{\mathrm{T}}(\mu + j) > 20\ \mathrm{GeV})/N(p_{\mathrm{T}}(j_\mu + j) > 20\ \mathrm{GeV})]$, which is evaluated from simulated top-quark events. The data sample includes background contributions from muons originating in intermediate τ decays, in addition to those produced directly in $W \to \mu\nu$ decays. To ensure that the reported cross sections correspond exclusively to prompt muons from W decays, a correction factor, defined as the fraction of such muons relative to the total, is derived from simulation and applied to the yields measured in data. The effect of the acceptance factor is found to be below 2%.

The sources of systematic uncertainties considered in the cross-section measurements are summarized in Table I. The dominant contribution arises from b-jet tagging, which comprises uncertainties from both the mistag fraction and the b-tagging efficiency. These are affected by common factors such as the choice of the parton-shower model (comparing MadGraph interfaced with Pythia and with Herwig, with kinematic weighting applied), variations in the simulated flavor composition (achieved by altering the fractions of light-flavor and c jets in the fit), and the jet energy scale and resolution effects (evaluated through smearing and scaling). For the mistag fraction, an additional contribution arises from the statistical precision of the template fits. For the b-tagging efficiency, the dominant statistical contribution comes from data-driven corrections, including the template fits and the weights based on the ratio of data to simulation. The second-largest systematic uncertainty originates from the jet energy scale and resolution. The efficiency of the $p_{\mathrm{T,jet}} > 50$ GeV requirement is evaluated in simulation. A control sample of Z + jet events is used to

TABLE II. Measured t- and $\bar{t}$-quark differential cross sections as a function of η_μ. Uncertainties are statistical, systematic, and from the luminosity, respectively.

η_μ interval	σ_t (pb)	$\sigma_{\bar{t}}$ (pb)
2.000–2.625	$0.722 \pm 0.040 \pm 0.063 \pm 0.014$	$0.653 \pm 0.035 \pm 0.055 \pm 0.013$
2.625–3.250	$0.507 \pm 0.033 \pm 0.043 \pm 0.010$	$0.437 \pm 0.030 \pm 0.037 \pm 0.009$
3.250–3.875	$0.234 \pm 0.022 \pm 0.019 \pm 0.005$	$0.173 \pm 0.020 \pm 0.016 \pm 0.003$
3.875–4.500	$0.061 \pm 0.014 \pm 0.008 \pm 0.001$	$0.044 \pm 0.012 \pm 0.007 \pm 0.001$

assess the energy scale and resolution as done in Ref. [88], which are then propagated to the top-quark simulation to evaluate the impact.

The uncertainty associated with the ABCD background estimation method receives contributions from several effects. The method assumes that the two discriminating variables are uncorrelated. To reduce possible correlations, the ratio N_C/N_A in the region $I_\mu < 0.9$ is calculated as a function of $p_{\mathrm{T}}^{j_\mu}$, and used to weight both the A and B samples following the strategy of Ref. [89]. The impact of this weighting is quantified by assessing the signal yield variations, with the difference assigned as the corresponding systematic uncertainty. In addition, the impact of the uncertainties on the correction coefficients is evaluated by varying each coefficient independently by $\pm 10\%$. The resulting variation in the extracted signal yield is taken as its systematic uncertainty.

The systematic uncertainty on the $Z + b$-jet background arises from the statistical uncertainty of the acceptance correction factor. The uncertainty of the $W + b$-jet background originates from uncertainties in the theoretical prediction of the NLO cross-section ratio $\sigma(W + b\,\mathrm{jet})/\sigma(W + \mathrm{jet})$. The effect of PDF uncertainties is determined using the technique of Monte Carlo PDF replicas, while the scale uncertainty is obtained from the envelope of variations where both the factorization and renormalization scales are independently varied up and down by a factor of two, as well as from the variation of the strong-coupling constant α_s [90].

Muon reconstruction uncertainties are derived from data-driven efficiency measurements using $Z \to \mu^+\mu^-$ events and applied to the simulated t-quark samples. The jet reconstruction uncertainty is similarly evaluated using $Z(\to \mu^+\mu^-) + \mathrm{jet}$ control samples. The uncertainty from the selection efficiency accounts for the limited size of the simulated t-quark samples. A 2% uncertainty is assigned to the integrated luminosity, as determined in Ref. [91]. The results obtained separately for the two magnet polarities are compatible within statistical uncertainties, and no additional systematic uncertainty is assigned.

TABLE III. Measured t-quark charge asymmetry as a function of η_μ. Uncertainties are statistical and systematic, respectively. The significance quantifies the deviation from zero.

η_μ range	A_C^t	Significance
2.000–2.625	$0.05 \pm 0.04 \pm 0.02$	1.22
2.625–3.250	$0.07 \pm 0.05 \pm 0.02$	1.44
3.250–3.875	$0.15 \pm 0.07 \pm 0.03$	1.91
3.875–4.500	$0.17 \pm 0.18 \pm 0.09$	0.85
2.0–4.5 (combined)	$0.08 \pm 0.03 \pm 0.01$	2.64

The integrated production cross sections for t and $\bar{t}$ are measured using Eq. (2) to be

$$\sigma_t = 0.95 \pm 0.04(\mathrm{stat}) \pm 0.08(\mathrm{syst}) \pm 0.02(\mathrm{lumi})\ \mathrm{pb},$$

$$\sigma_{\bar{t}} = 0.81 \pm 0.03(\mathrm{stat}) \pm 0.07(\mathrm{syst}) \pm 0.02(\mathrm{lumi})\ \mathrm{pb},$$

where the quoted uncertainties are statistical, systematic, and from the luminosity determination, respectively. The systematic uncertainties of the t and $\bar{t}$ cross sections are correlated at the level of 96%. The inclusive charge asymmetry is measured as

$$A_C^t = 0.08 \pm 0.03(\mathrm{stat}) \pm 0.01(\mathrm{syst}).$$

Differential cross sections and charge asymmetries as a function of η_μ are shown in Figs. 1 and 2, and summarized in Tables II and III. The measurements are compared with NLO predictions from Powheg-BOX [92] using CT18 [93] and NNPDF31 [94] PDFs and MadGraph [79] using NNPDF31, and good agreement is observed. Theoretical uncertainties contain the PDF, scale, and α_s uncertainties [95].

In summary, the first measurement of the top-quark charge asymmetry and the differential t- and $\bar{t}$-quark production cross sections in the forward region is presented, using pp collisions collected with the LHCb detector between 2015 and 2018 at $\sqrt{s} = 13$ TeV, corresponding to an integrated luminosity of 5.4 fb^{-1}. The results represent the most precise top-quark production cross-section measurements in the forward region to date.

For the charge asymmetry measurement, the $\mu + b$-jet final state receives contributions from both $t\bar{t}$ and single-top production. In future analyses with larger data sets, the measured asymmetry should be decomposed through a fit incorporating the expected asymmetries from both processes.

Acknowledgments—We express our gratitude to our colleagues in the CERN accelerator departments for the excellent performance of the LHC. We thank the technical

and administrative staff at the LHCb institutes. We thank James Vincent Mead and Stephen Farry for their pioneering work on top-quark production, which has substantially informed and supported the development of this measurement [96]. We acknowledge support from CERN and from the national agencies: ARC (Australia); CAPES, CNPq, FAPERJ and FINEP (Brazil); MOST and NSFC (China); CNRS/IN2P3 (France); BMFTR, DFG and MPG (Germany); INFN (Italy); NWO (Netherlands); MNiSW and NCN (Poland); MCID/IFA (Romania); MICIU and AEI (Spain); SNSF and SER (Switzerland); NASU (Ukraine); STFC (United Kingdom); DOE NP and NSF (USA). We acknowledge the computing resources that are provided by ARDC (Australia), CBPF (Brazil), CERN, IHEP and LZU (China), IN2P3 (France), KIT and DESY (Germany), INFN (Italy), SURF (Netherlands), Polish WLCG (Poland), IFIN-HH (Romania), PIC (Spain), CSCS (Switzerland), and GridPP (United Kingdom). We are indebted to the communities behind the multiple open-source software packages on which we depend. Individual groups or members have received support from Key Research Program of Frontier Sciences of CAS, CAS PIFI, CAS CCEPP, Minciencias (Colombia); EPLANET, Marie Skłodowska-Curie Actions, ERC and NextGenerationEU (European Union); A*MIDEX, ANR, IPhU and Labex P2IO, and Région Auvergne-Rhône-Alpes (France); Alexander-von-Humboldt Foundation (Germany); ICSC (Italy); Severo Ochoa and María de Maeztu Units of Excellence, GVA, XuntaGal, GENCAT, InTalent-Inditex and Prog. Atracción Talento CM (Spain); SRC (Sweden); the Leverhulme Trust, the Royal Society and UKRI (United Kingdom).

Data availability—Data associated to the plots in this publication are made available on the CERN Document Server in Ref. [97].

[1] S. Navas *et al.* (Particle Data Group), Review of particle physics, Phys. Rev. D **110**, 030001 (2024).
[2] A. L. Kagan, J. F. Kamenik, G. Perez, and S. Stone, Probing new top physics at the LHCb experiment, Phys. Rev. Lett. **107**, 082003 (2011).
[3] R. Gauld, Feasibility of top quark measurements at LHCb and constraints on the large-x gluon PDF, J. High Energy Phys. 02 (2014) 126.
[4] R. Gauld, Leptonic top quark asymmetry predictions at LHCb, Phys. Rev. D **91**, 054029 (2015).
[5] J. M. Campbell, R. K. Ellis, P. Nason, and E. Re, Top-pair production and decay at NLO matched with parton showers, J. High Energy Phys. 04 (2015) 114.
[6] S. Alioli, P. Nason, C. Oleari, and E. Re, NLO single-top production matched with shower in Powheg: s- and t-channel contributions, J. High Energy Phys. 09 (2009) 111.
[7] E. Re, Single-top Wt-channel production matched with parton showers using the Powheg method, Eur. Phys. J. C **71**, 1547 (2011).
[8] M. Czakon, M. L. Mangano, A. Mitov, and J. Rojo, Constraints on the gluon PDF from top quark pair production at hadron colliders, J. High Energy Phys. 07 (2013) 167.
[9] S. Alekhin, M. V. Garzelli, S.-O. Moch, and O. Zenaiev, NNLO PDFs driven by top-quark data, Eur. Phys. J. C **85**, 162 (2025).
[10] A. Ablat, M. Guzzi, K. Xie, S. Dulat, T.-J. Hou, I. Sitiwaldi, and C.-P. Yuan, Exploring the impact of high-precision top-quark pair production data on the structure of the proton at the LHC, Phys. Rev. D **109**, 054027 (2024).
[11] W. Bernreuther and Z.-G. Si, Top quark and leptonic charge asymmetries for the Tevatron and LHC, Phys. Rev. D **86**, 034026 (2012).
[12] S. Chatrchyan *et al.* (CMS Collaboration), Measurement of the $t\bar{t}$ production cross section in pp collisions at $\sqrt{s} =$ 7 TeV with lepton + jets final states, Phys. Lett. B **720**, 83 (2013).
[13] S. Chatrchyan *et al.* (CMS Collaboration), Measurement of the single-top-quark t-channel cross section in pp collisions at $\sqrt{s} = 7$ TeV, J. High Energy Phys. 12 (2012) 035.
[14] S. Chatrchyan *et al.* (CMS Collaboration), Measurement of the $t\bar{t}$ production cross section in the all-jet final state in pp collisions at $\sqrt{s} = 7$ TeV, J. High Energy Phys. 05 (2013) 065.
[15] G. Aad *et al.* (ATLAS Collaboration), Comprehensive measurements of t-channel single top-quark production cross sections at $\sqrt{s} = 7$ TeV with the ATLAS detector, Phys. Rev. D **90**, 112006 (2014).
[16] V. Khachatryan *et al.* (CMS Collaboration), Measurement of the t-channel single-top-quark production cross section and of the $|V_{tb}|$ CKM matrix element in pp collisions at $\sqrt{s} = 8$ TeV, J. High Energy Phys. 06 (2014) 090.
[17] G. Aad *et al.* (ATLAS Collaboration), Measurement of the $t\bar{t}$ production cross-section using $e\mu$ events with b-tagged jets in pp collisions at $\sqrt{s} = 7$ and 8 TeV with the ATLAS detector, Eur. Phys. J. C **74**, 3109 (2014); **76**, 642(A) (2016).
[18] V. Khachatryan *et al.* (CMS Collaboration), Measurement of the $t\bar{t}$ production cross section in the all-jets final state in pp collisions at $\sqrt{s} = 8$ TeV, Eur. Phys. J. C **76**, 128 (2016).
[19] M. Aaboud *et al.* (ATLAS Collaboration), Measurement of the inclusive cross-sections of single top-quark and top-antiquark t-channel production in pp collisions at $\sqrt{s} =$ 13 TeV with the ATLAS detector, J. High Energy Phys. 04 (2017) 086.
[20] V. Khachatryan *et al.* (CMS Collaboration), Measurement of the $t\bar{t}$ production cross section in the $e\mu$ channel in proton-proton collisions at $\sqrt{s} = 7$ and 8 TeV, J. High Energy Phys. 08 (2016) 029.
[21] V. Khachatryan *et al.* (CMS Collaboration), Measurements of the $t\bar{t}$ production cross section in lepton + jets final states in pp collisions at 8 TeV and ratio of 8 to 7 TeV cross sections, Eur. Phys. J. C **77**, 15 (2017).
[22] M. Aaboud *et al.* (ATLAS Collaboration), Measurement of the $t\bar{t}$ production cross section in the τ + jets final state in pp collisions at $\sqrt{s} = 8$ TeV using the ATLAS detector, Phys. Rev. D **95**, 072003 (2017).
[23] M. Aaboud *et al.* (ATLAS Collaboration), Measurement of the inclusive and fiducial $t\bar{t}$ production cross-sections in the

lepton + jets channel in pp collisions at $\sqrt{s} = 8$ TeV with the ATLAS detector, Eur. Phys. J. C **78**, 487 (2018).
[24] M. Aaboud *et al.* (ATLAS Collaboration), Fiducial, total and differential cross-section measurements of t-channel single top-quark production in pp collisions at 8 TeV using data collected by the ATLAS detector, Eur. Phys. J. C **77**, 531 (2017).
[25] A. M. Sirunyan *et al.* (CMS Collaboration), Measurement of the $t\bar{t}$ production cross section, the top quark mass, and the strong coupling constant using dilepton events in pp collisions at $\sqrt{s} = 13$ TeV, Eur. Phys. J. C **79**, 368 (2019).
[26] A. M. Sirunyan *et al.* (CMS Collaboration), Measurement of the single top quark and antiquark production cross sections in the t channel and their ratio in proton-proton collisions at $\sqrt{s} = 13$ TeV, Phys. Lett. B **800**, 135042 (2020).
[27] A. M. Sirunyan *et al.* (CMS Collaboration), Measurement of the top quark pair production cross section in dilepton final states containing one τ lepton in pp collisions at $\sqrt{s} = 13$ TeV, J. High Energy Phys. 02 (2020) 191.
[28] G. Aad *et al.* (ATLAS Collaboration), Measurements of top-quark pair single- and double-differential cross-sections in the all-hadronic channel in pp collisions at $\sqrt{s} = 13$ TeV using the ATLAS detector, J. High Energy Phys. 01 (2021) 033.
[29] A. Tumasyan *et al.* (CMS Collaboration), Measurement of the inclusive $t\bar{t}$ production cross section in proton-proton collisions at $\sqrt{s} = 5.02$ TeV, J. High Energy Phys. 04 (2022) 144.
[30] A. Tumasyan *et al.* (CMS Collaboration), Measurement of differential $t\bar{t}$ production cross sections in the full kinematic range using lepton + jets events from proton-proton collisions at $\sqrt{s} = 13$ TeV, Phys. Rev. D **104**, 092013 (2021).
[31] G. Aad *et al.* (ATLAS, CMS Collaborations), Combination of inclusive top-quark pair production cross-section measurements using ATLAS and CMS data at $\sqrt{s} = 7$ and 8 TeV, J. High Energy Phys. 07 (2023) 213.
[32] G. Aad *et al.* (ATLAS Collaboration), Measurement of the $t\bar{t}$ production cross-section in pp collisions at $\sqrt{s} = 5.02$ TeV with the ATLAS detector, J. High Energy Phys. 06 (2023) 138.
[33] M. Aaboud *et al.* (ATLAS Collaboration), Measurement of the inclusive $t\bar{t}$ production cross section in the lepton + jets channel in pp collisions at $\sqrt{s} = 7$ TeV with the ATLAS detector using support vector machines, Phys. Rev. D **108**, 032014 (2023).
[34] G. Aad *et al.* (ATLAS Collaboration), Inclusive and differential cross-sections for dilepton $t\bar{t}$ production measured in $\sqrt{s} = 13$ TeV pp collisions with the ATLAS detector, J. High Energy Phys. 07 (2023) 141.
[35] G. Aad *et al.* (ATLAS Collaboration), Measurement of the $t\bar{t}$ cross section and its ratio to the Z production cross section using pp collisions at $\sqrt{s} = 13.6$ TeV with the ATLAS detector, Phys. Lett. B **848**, 138376 (2024).
[36] A. Tumasyan *et al.* (CMS Collaboration), First measurement of the top quark pair production cross section in proton-proton collisions at $\sqrt{s} = 13.6$ TeV, J. High Energy Phys. 08 (2023) 204.
[37] A. Hayrapetyan *et al.* (CMS Collaboration), Measurement of the inclusive $t\bar{t}$ cross section in final states with at least one lepton and additional jets with 302 pb^{-1} of pp collisions at $\sqrt{s} = 5.02$ TeV, J. High Energy Phys. 04 (2025) 099.
[38] R. Aaij *et al.* (LHCb Collaboration), First observation of top quark production in the forward region, Phys. Rev. Lett. **115**, 112001 (2015).
[39] R. Aaij *et al.* (LHCb Collaboration), Measurement of forward $t\bar{t}$, $W + b\bar{b}$ and $W + c\bar{c}$ production in $p\,p$ collisions at $\sqrt{s} = 8$ TeV, Phys. Lett. B **767**, 110 (2017).
[40] R. Aaij *et al.* (LHCb Collaboration), Measurement of forward top pair production in the dilepton channel in $p\,p$ collisions at $\sqrt{s} = 13$ TeV, J. High Energy Phys. 08 (2018) 174.
[41] T. Aaltonen *et al.* (CDF Collaboration), Evidence for a mass dependent forward-backward asymmetry in top quark pair production, Phys. Rev. D **83**, 112003 (2011).
[42] V. M. Abazov *et al.* (D0 Collaboration), Simultaneous measurement of forward-backward asymmetry and top polarization in dilepton final states from $t\bar{t}$ production at the Tevatron, Phys. Rev. D **92**, 052007 (2015).
[43] T. Aaltonen *et al.* (CDF Collaboration), Measurement of the top quark forward-backward production asymmetry and its dependence on event kinematic properties, Phys. Rev. D **87**, 092002 (2013).
[44] M. Czakon, P. Fiedler, and A. Mitov, Resolving the Tevatron top quark forward-backward asymmetry puzzle: Fully differential next-to-next-to-leading-order calculation, Phys. Rev. Lett. **115**, 052001 (2015).
[45] V. M. Abazov *et al.* (D0 Collaboration), Measurement of the forward-backward asymmetry in top quark-antiquark production in $p\bar{p}$ collisions using the lepton + jets channel, Phys. Rev. D **90**, 072011 (2014).
[46] N. Kidonakis, Top quark forward-backward asymmetry at approximate N^3LO, Phys. Rev. D **91**, 071502(R) (2015).
[47] T. A. Aaltonen *et al.* (CDF, D0 Collaborations), Combined forward-backward asymmetry measurements in top-antitop quark production at the Tevatron, Phys. Rev. Lett. **120**, 042001 (2018).
[48] G. Aad *et al.* (ATLAS Collaboration), Measurement of the top quark pair production charge asymmetry in proton-proton collisions at $\sqrt{s} = 7$ TeV using the ATLAS detector, J. High Energy Phys. 02 (2014) 107.
[49] G. Aad *et al.* (ATLAS Collaboration), Measurement of the charge asymmetry in dileptonic decays of top quark pairs in pp collisions at $\sqrt{s} = 7$ TeV using the ATLAS detector, J. High Energy Phys. 05 (2015) 061.
[50] G. Aad *et al.* (ATLAS Collaboration), Measurement of the charge asymmetry in top-quark pair production in the lepton-plus-jets final state in pp collision data at $\sqrt{s} =$ 8 TeV with the ATLAS detector, Eur. Phys. J. C **76**, 87 (2016); **77**, 564(E) (2017).
[51] G. Aad *et al.* (ATLAS Collaboration), Measurement of the charge asymmetry in highly boosted top-quark pair production in $\sqrt{s} = 8$ TeV pp collision data collected by the ATLAS experiment, Phys. Lett. B **756**, 52 (2016).
[52] G. Aad *et al.* (ATLAS Collaboration), Measurement of the charge asymmetry in top-quark pair production in association with a photon with the ATLAS experiment, Phys. Lett. B **843**, 137848 (2023).
[53] G. Aad *et al.* (ATLAS Collaboration), Evidence for the charge asymmetry in pp $\rightarrow t\bar{t}$ production at $\sqrt{s} = 13$ TeV with the ATLAS detector, J. High Energy Phys. 08 (2023) 077.

[54] S. Chatrchyan *et al.* (CMS Collaboration), Inclusive and differential measurements of the $t\bar{t}$ charge asymmetry in proton-proton collisions at $\sqrt{s} = 7$ TeV, Phys. Lett. B **717**, 129 (2012).

[55] S. Chatrchyan *et al.* (CMS Collaboration), Measurements of the $t\bar{t}$ charge asymmetry using the dilepton decay channel in pp collisions at $\sqrt{s} = 7$ TeV, J. High Energy Phys. 04 (2014) 191.

[56] V. Khachatryan *et al.* (CMS Collaboration), Measurement of the charge asymmetry in top quark pair production in pp collisions at $\sqrt{s} = 8$ TeV using a template method, Phys. Rev. D **93**, 034014 (2016).

[57] V. Khachatryan *et al.* (CMS Collaboration), Inclusive and differential measurements of the $t\bar{t}$ charge asymmetry in pp collisions at $\sqrt{s} = 8$ TeV, Phys. Lett. B **757**, 154 (2016).

[58] V. Khachatryan *et al.* (CMS Collaboration), Measurements of $t\bar{t}$ charge asymmetry using dilepton final states in pp collisions at $\sqrt{s} = 8$ TeV, Phys. Lett. B **760**, 365 (2016).

[59] Charge-conjugate states are implied throughout this Letter.

[60] Natural units with $\hbar = c = 1$ are used throughout.

[61] M. Cacciari, G. P. Salam, and G. Soyez, The anti-k_t jet clustering algorithm, J. High Energy Phys. 04 (2008) 063.

[62] R. Aaij *et al.* (LHCb Collaboration), Study of forward $Z +$ jet production in $p\ p$ collisions at $\sqrt{s} = 7$ TeV, J. High Energy Phys. 01 (2014) 033.

[63] A. A. Alves Jr. *et al.* (LHCb Collaboration), The LHCb detector at the LHC, J. Instrum. **3**, S08005 (2008).

[64] LHCb Collaboration, LHCb detector performance, Int. J. Mod. Phys. A **30**, 1530022 (2015).

[65] R. Aaij *et al.*, Performance of the LHCb Vertex Locator, J. Instrum. **9**, P09007 (2014).

[66] P. d'Argent *et al.*, Improved performance of the LHCb Outer Tracker in LHC Run 2, J. Instrum. **12**, P11016 (2017).

[67] M. Adinolfi *et al.*, Performance of the LHCb RICH detector at the LHC, Eur. Phys. J. C **73**, 2431 (2013).

[68] A. A. Alves Jr. *et al.*, Performance of the LHCb muon system, J. Instrum. **8**, P02022 (2013).

[69] R. Aaij *et al.*, The LHCb trigger and its performance in 2011, J. Instrum. **8**, P04022 (2013).

[70] R. Aaij *et al.*, Design and performance of the LHCb trigger and full real-time reconstruction in Run 2 of the LHC, J. Instrum. **14**, P04013 (2019).

[71] T. Sjöstrand, S. Mrenna, and P. Skands, A brief introduction to Pythia 8.1, Comput. Phys. Commun. **178**, 852 (2008).

[72] I. Belyaev *et al.*, Handling of the generation of primary events in Gauss, the LHCb simulation framework, J. Phys. Conf. Ser. **331**, 032047 (2011).

[73] N. Davidson, T. Przedzinski, and Z. Was, Photos interface in C++: Technical and physics documentation, Comput. Phys. Commun. **199**, 86 (2016).

[74] J. Allison *et al.* (Geant4 Collaboration), Geant4 developments and applications, IEEE Trans. Nucl. Sci. **53**, 270 (2006); S. Agostinelli *et al.* (Geant4 Collaboration), Geant4: A simulation toolkit, Nucl. Instrum. Methods Phys. Res., Sect. A **506**, 250 (2003).

[75] M. Clemencic, G. Corti, S. Easo, C. R. Jones, S. Miglioranzi, M. Pappagallo, and P. Robbe, The LHCb simulation application, Gauss: Design, evolution and experience, J. Phys. Conf. Ser. **331**, 032023 (2011).

[76] P. Nason, A new method for combining NLO QCD with shower Monte Carlo algorithms, J. High Energy Phys. 11 (2004) 040.

[77] S. Frixione, P. Nason, and C. Oleari, Matching NLO QCD computations with parton shower simulations: The Powheg method, J. High Energy Phys. 11 (2007) 070.

[78] S. Alioli, P. Nason, C. Oleari, and E. Re, A general framework for implementing NLO calculations in shower Monte Carlo programs: The Powheg BOX, J. High Energy Phys. 06 (2010) 043.

[79] J. Alwall, R. Frederix, S. Frixione, V. Hirschi, F. Maltoni, O. Mattelaer, H.-S. Shao, T. Stelzer, P. Torrielli, and M. Zaro, The automated computation of tree-level and next-to-leading order differential cross sections, and their matching to parton shower simulations, J. High Energy Phys. 07 (2014) 079.

[80] R. Aaij *et al.* (LHCb Collaboration), Measurement of forward W and Z boson production in association with jets in proton-proton collisions at $\sqrt{s} = 8$ TeV, J. High Energy Phys. 05 (2016) 131.

[81] E. Bols, J. Kieseler, M. Verzetti, M. Stoye, and A. Stakia, Jet flavour classification using DeepJet, J. Instrum. **15**, P12012 (2020).

[82] R. Aaij *et al.* (LHCb Collaboration), Search for $H \to b\bar{b}$ and $H \to c\bar{c}$ in $\sqrt{s} = 13$ TeV pp collisions at LHCb using machine learning techniques, LHCb-PAPER-2025-034, arXiv:2601.16802.

[83] G. Aad *et al.* (ATLAS Collaboration), Measurement of the inclusive isolated prompt photon cross section in pp collisions at $\sqrt{s} = 7$ TeV with the ATLAS detector, Phys. Rev. D **83**, 052005 (2011).

[84] R. Aaij *et al.* (LHCb Collaboration), Precision measurement of forward Z boson production in proton-proton collisions at $\sqrt{s} = 13$ TeV, J. High Energy Phys. 07 (2022) 026.

[85] R. Aaij *et al.* (LHCb Collaboration), Measurement of the forward W boson production cross-section in $p\ p$ collisions at $\sqrt{s} = 7$ TeV, J. High Energy Phys. 12 (2014) 079.

[86] R. Aaij *et al.* (LHCb Collaboration), Measurement of the forward Z boson cross-section in $p\ p$ collisions at $\sqrt{s} = 7$ TeV, J. High Energy Phys. 08 (2015) 039.

[87] R. Aaij *et al.* (LHCb Collaboration), Measurement of forward W and Z boson production in $p\ p$ collisions at $\sqrt{s} = 8$ TeV, J. High Energy Phys. 01 (2016) 155.

[88] R. Aaij *et al.* (LHCb Collaboration), Measurement of differential $b\bar{b}$ and $c\bar{c}$ dijet cross-sections in the forward region of pp collisions at $\sqrt{s} = 13$ TeV, J. High Energy Phys. 02 (2021) 023.

[89] R. Aaij *et al.* (LHCb Collaboration), Study of W boson production in association with beauty and charm, Phys. Rev. D **92**, 052001 (2015).

[90] S. Dittmaier *et al.* (LHC Higgs Cross Section Working Group), Handbook of LHC Higgs cross sections: 1. inclusive observables, 10.5170/CERN-2011-002.

[91] LHCb Collaboration, Precision luminosity measurements at LHCb, J. Instrum. **9**, P12005 (2014).

[92] T. Ježo and P. Nason, On the treatment of resonances in next-to-leading order calculations matched to a parton shower, J. High Energy Phys. 12 (2015) 065.

[93] T.-J. Hou *et al.*, New CTEQ global analysis of quantum chromodynamics with high-precision data from the LHC, Phys. Rev. D **103**, 014013 (2021).

[94] R. D. Ball *et al.* (NNPDF Collaboration), Parton distributions from high-precision collider data, Eur. Phys. J. C **77**, 663 (2017).

[95] D. Bourilkov, R. C. Group, and M. R. Whalley, LHAPDF: PDF use from the Tevatron to the LHC, in *TeV4LHC Workshop—4th Meeting* (2006), arXiv:hep-ph/0605240.

[96] J. V. Mead, A measurement of top quark production at $\sqrt{s} =$ 13 TeV with LHCb data, CERN-THESIS-2021-130, 2021, https://cds.cern.ch/record/2780780.

[97] LHCb Collaboration, Measurement of the top-quark production cross-section and charge asymmetry at LHCb, LHCb-PAPER-2025-057-cds, https://cds.cern.ch/record/2951095.

End Matter

For the differential cross-section measurement, the correlation matrix is constructed by evaluating the shift in each bin associated with each systematic variation. Uncertainties related to muon identification, tracking, trigger efficiencies, jet reconstruction efficiency, event selection efficiency, and the statistical components of the b-jet tagging efficiency are treated using the rms method, which quantifies their statistical spread by computing the root-mean-square of the resulting cross section shifts across all variations. For uncertainties arising from the ABCD method, background estimation method, the jet energy scale and resolution, and the components of the b-jet tagging systematics whose variations are intrinsic to the methodology itself, the envelope method is employed. In this approach, the largest absolute deviation among all variations is taken as the systematic uncertainty, and the correlations across bins are assumed to be 100%. The correlation matrix for the differential cross-section measurements is presented in Table IV. Owing to the limited statistics in the last bin, the systematic uncertainties have large fluctuations. This statistical limitation leads to the appearance of the small correlation in the correlation matrix.

TABLE IV. Correlation matrix for the systematic uncertainties in the differential cross-section measurements of t and $\bar{t}$ quarks as a function of η_μ. Bins 1–4 correspond to $\bar{t}$ (η_{μ^-}) and bins 5–8 to t (η_{μ^+}). The luminosity uncertainty, fully correlated across all bins, is excluded.

	$\sigma_{\bar{t}}$ (η_{μ^-})				σ_t (η_{μ^+})			
Bin index	1	2	3	4	5	6	7	8
1	1.00							
2	0.88	1.00						
3	0.83	0.68	1.00					
4	0.27	0.48	0.59	1.00				
5	0.93	0.98	0.73	0.42	1.00			
6	0.97	0.89	0.90	0.44	0.93	1.00		
7	0.84	0.96	0.79	0.67	0.93	0.91	1.00	
8	0.77	0.90	0.42	0.16	0.88	0.75	0.79	1.00

R. Aaij,[38] A. S. W. Abdelmotteleb,[58] C. Abellan Beteta,[52] F. Abudinén,[60] T. Ackernley,[62] A. A. Adefisoye,[70] B. Adeva,[48] M. Adinolfi,[56] P. Adlarson,[86] C. Agapopoulou,[14] C. A. Aidala,[88] Z. Ajaltouni,[11] S. Akar,[11] K. Akiba,[38] M. Akthar,[40] P. Albicocco,[28] J. Albrecht,[19,b] R. Aleksiejunas,[82] F. Alessio,[50] P. Alvarez Cartelle,[57,48] R. Amalric,[16] S. Amato,[3] J. L. Amey,[56] Y. Amhis,[14] L. An,[6] L. Anderlini,[27] M. Andersson,[52] P. Andreola,[52] M. Andreotti,[26] S. Andres Estrada,[45] A. Anelli,[31,c] D. Ao,[7] C. Arata,[12] F. Archilli,[37] Z. Areg,[70] M. Argenton,[26] S. Arguedas Cuendis,[9,50] L. Arnone,[31,c] A. Artamonov,[44] M. Artuso,[70] E. Aslanides,[13] R. Ataíde Da Silva,[51] M. Atzeni,[66] B. Audurier,[12] J. A. Authier,[15] D. Bacher,[65] I. Bachiller Perea,[51] S. Bachmann,[22] M. Bachmayer,[51] J. J. Back,[58] P. Baladron Rodriguez,[48] V. Balagura,[15] A. Balboni,[26] W. Baldini,[26] Z. Baldwin,[80] L. Balzani,[19] H. Bao,[7] J. Baptista de Souza Leite,[2] C. Barbero Pretel,[48,12] M. Barbetti,[27] I. R. Barbosa,[71] R. J. Barlow,[64,a] M. Barnyakov,[25] S. Barsuk,[14] W. Barter,[60] J. Bartz,[70] S. Bashir,[40] B. Batsukh,[5] P. B. Battista,[14] A. Bavarchee,[81] A. Bay,[51] A. Beck,[66] M. Becker,[19] F. Bedeschi,[35] I. B. Bediaga,[2] N. A. Behling,[19] S. Belin,[48] A. Bellavista,[25] K. Belous,[44] I. Belov,[29] I. Belyaev,[36] G. Benane,[13] G. Bencivenni,[28] E. Ben-Haim,[16]

A. Berezhnoy,[44] R. Bernet,[52] S. Bernet Andres,[47] A. Bertolin,[33] F. Betti,[60] J. Bex,[57] O. Bezshyyko,[87] S. Bhattacharya,[81] M. S. Bieker,[18] N. V. Biesuz,[26] A. Biolchini,[38] M. Birch,[63] F. C. R. Bishop,[10] A. Bitadze,[64] A. Bizzeti,[27,d] T. Blake,[58,e] F. Blanc,[51] J. E. Blank,[19] S. Blusk,[70] V. Bocharnikov,[44] J. A. Boelhauve,[19] O. Boente Garcia,[50] T. Boettcher,[89] A. Bohare,[60] A. Boldyrev,[44] C. Bolognani,[84] R. Bolzonella,[26,f] R. B. Bonacci,[1] N. Bondar,[44,50] A. Bordelius,[50] F. Borgato,[33,50] S. Borghi,[64] M. Borsato,[31,c] J. T. Borsuk,[85] E. Bottalico,[62] S. A. Bouchiba,[51] M. Bovill,[65] T. J. V. Bowcock,[62] A. Boyer,[50] C. Bozzi,[26] J. D. Brandenburg,[90] A. Brea Rodriguez,[51] N. Breer,[19] J. Brodzicka,[41] J. Brown,[62] D. Brundu,[32] E. Buchanan,[60] M. Burgos Marcos,[84] C. Burr,[50] C. Buti,[27] J. S. Butter,[57] J. Buytaert,[50] W. Byczynski,[50] S. Cadeddu,[32] H. Cai,[76] Y. Cai,[5] A. Caillet,[16] R. Calabrese,[26,f] L. Calefice,[46] M. Calvi,[31,c] M. Calvo Gomez,[47] P. Camargo Magalhaes,[2,g] J. I. Cambon Bouzas,[48] P. Campana,[28] A. C. Campos,[3] A. F. Campoverde Quezada,[7] Y. Cao,[6] S. Capelli,[31] M. Caporale,[25] L. Capriotti,[26] R. Caravaca-Mora,[9] A. Carbone,[25,h] L. Carcedo Salgado,[48] R. Cardinale,[29,i] A. Cardini,[32] P. Carniti,[31] L. Carus,[22] A. Casais Vidal,[66] R. Caspary,[22] G. Casse,[62] M. Cattaneo,[50] G. Cavallero,[26] V. Cavallini,[26,f] S. Celani,[50] I. Celestino,[35,j] S. Cesare,[50,k] A. J. Chadwick,[62] I. Chahrour,[88] H. Chang,[4,l] M. Charles,[16] Ph. Charpentier,[50] E. Chatzianagnostou,[38] R. Cheaib,[81] M. Chefdeville,[10] C. Chen,[57] J. Chen,[51] S. Chen,[5] Z. Chen,[7] A. Chen Hu,[63] M. Cherif,[12] A. Chernov,[41] S. Chernyshenko,[54] X. Chiotopoulos,[84] V. Chobanova,[45] M. Chrzaszcz,[41] A. Chubykin,[44] V. Chulikov,[28,50,36] P. Ciambrone,[28] X. Cid Vidal,[48] G. Ciezarek,[50] P. Cifra,[50] P. E. L. Clarke,[60] M. Clemencic,[50] H. V. Cliff,[57] J. Closier,[50] C. Cocha Toapaxi,[22] V. Coco,[50] J. Cogan,[13] E. Cogneras,[11] L. Cojocariu,[43] S. Collaviti,[51] P. Collins,[50] T. Colombo,[50] M. Colonna,[19] A. Comerma-Montells,[46] L. Congedo,[24] J. Connaughton,[58] A. Contu,[32] N. Cooke,[61] G. Cordova,[35,j] C. Coronel,[67] I. Corredoira,[12] A. Correia,[16] G. Corti,[50] J. Cottee Meldrum,[56] B. Couturier,[50] D. C. Craik,[52] M. Cruz Torres,[2,m] M. Cubero Campos,[9] E. Curras Rivera,[51] R. Currie,[60] C. L. Da Silva,[69] S. Dadabaev,[44] X. Dai,[4] E. Dall'Occo,[50] J. Dalseno,[45] C. D'Ambrosio,[63] J. Daniel,[11] G. Darze,[3] A. Davidson,[58] J. E. Davies,[64] O. De Aguiar Francisco,[64] C. De Angelis,[32,n] F. De Benedetti,[50] J. de Boer,[38] K. De Bruyn,[83] S. De Capua,[64] M. De Cian,[64,50] U. De Freitas Carneiro Da Graca,[2,o] E. De Lucia,[28] J. M. De Miranda,[2] L. De Paula,[3] M. De Serio,[24,p] P. De Simone,[28] F. De Vellis,[19] J. A. de Vries,[84] F. Debernardis,[24] D. Decamp,[10] S. Dekkers,[1] L. Del Buono,[16] B. Delaney,[66] J. Deng,[8] V. Denysenko,[52] O. Deschamps,[11] F. Dettori,[32,n] B. Dey,[81] P. Di Nezza,[28] I. Diachkov,[44] S. Didenko,[44] S. Ding,[70] Y. Ding,[51] L. Dittmann,[22] V. Dobishuk,[54] A. D. Docheva,[61] A. Doheny,[58] C. Dong,[4,l] F. Dordei,[32] A. C. dos Reis,[2] A. D. Dowling,[70] L. Dreyfus,[13] W. Duan,[74] P. Duda,[85] L. Dufour,[51] V. Duk,[34] P. Durante,[50] M. M. Duras,[85] J. M. Durham,[69] O. D. Durmus,[81] A. Dziurda,[41] A. Dzyuba,[44] S. Easo,[59] E. Eckstein,[18] U. Egede,[1] A. Egorychev,[44] V. Egorychev,[44] S. Eisenhardt,[60] E. Ejopu,[62] L. Eklund,[86] M. Elashri,[67] D. Elizondo Blanco,[9] J. Ellbracht,[19] S. Ely,[63] A. Ene,[43] J. Eschle,[70] T. Evans,[38] F. Fabiano,[14] S. Faghih,[67] L. N. Falcao,[31,c] B. Fang,[7] R. Fantechi,[35] L. Fantini,[34,q] M. Faria,[51] K. Farmer,[60] F. Fassin,[83,38] D. Fazzini,[31,c] L. Felkowski,[85] C. Feng,[6] M. Feng,[5,7] A. Fernandez Casani,[49] M. Fernandez Gomez,[48] A. D. Fernez,[68] F. Ferrari,[25,h] F. Ferreira Rodrigues,[3] M. Ferrillo,[52] M. Ferro-Luzzi,[50] S. Filippov,[44] R. A. Fini,[24] M. Fiorini,[26,f] M. Firlej,[40] K. L. Fischer,[65] D. S. Fitzgerald,[88] C. Fitzpatrick,[64] T. Fiutowski,[40] F. Fleuret,[15] A. Fomin,[53] M. Fontana,[25,50] L. A. Foreman,[64] R. Forty,[50] D. Foulds-Holt,[60] V. Franco Lima,[3] M. Franco Sevilla,[68] M. Frank,[50] E. Franzoso,[26,f] G. Frau,[64] C. Frei,[50] D. A. Friday,[64,50] J. Fu,[7] Q. Führing,[19,57,b] T. Fulghesu,[13] G. Galati,[24,p] M. D. Galati,[38] A. Gallas Torreira,[48] D. Galli,[25,h] S. Gambetta,[60] M. Gandelman,[3] P. Gandini,[30] B. Ganie,[64] H. Gao,[7] R. Gao,[65] T. Q. Gao,[57] Y. Gao,[8] Y. Gao,[6] Y. Gao,[8] L. M. Garcia Martin,[51] P. Garcia Moreno,[46] J. García Pardiñas,[66] P. Gardner,[68] L. Garrido,[46] C. Gaspar,[50] A. Gavrikov,[33] L. L. Gerken,[19] E. Gersabeck,[20] M. Gersabeck,[20] T. Gershon,[58] S. Ghizzo,[29,i] Z. Ghorbanimoghaddam,[56] F. I. Giasemis,[16,r] V. Gibson,[57] H. K. Giemza,[42] A. L. Gilman,[67] M. Giovannetti,[28] A. Gioventù,[46] L. Girardey,[64,59] M. A. Giza,[41] F. C. Glaser,[22,14] V. V. Gligorov,[16] C. Göbel,[71] L. Golinka-Bezshyyko,[87] E. Golobardes,[47] D. Golubkov,[44] A. Golutvin,[63,50] S. Gomez Fernandez,[46] W. Gomulka,[40] F. Goncalves Abrantes,[65] I. Gonçales Vaz,[50] M. Goncerz,[41] G. Gong,[4,l] J. A. Gooding,[19] I. V. Gorelov,[44] C. Gotti,[31] E. Govorkova,[66] J. P. Grabowski,[30] L. A. Granado Cardoso,[50] E. Graugés,[46] E. Graverini,[35,51,s] L. Grazette,[58] G. Graziani,[27] A. T. Grecu,[43] N. A. Grieser,[67] L. Grillo,[61] S. Gromov,[44] C. Gu,[15] M. Guarise,[26] L. Guerry,[11] A.-K. Guseinov,[51] E. Gushchin,[44] Y. Guz,[6,50] T. Gys,[50] K. Habermann,[18] T. Hadavizadeh,[1] C. Hadjivasiliou,[68] G. Haefeli,[51]

C. Haen,[50] S. Haken,[57] G. Hallett,[58] P. M. Hamilton,[68] J. Hammerich,[62] Q. Han,[33] X. Han,[22,50] S. Hansmann-Menzemer,[22] L. Hao,[7] N. Harnew,[65] T. J. Harris,[1] M. Hartmann,[14] S. Hashmi,[40] J. He,[7,t] N. Heatley,[14] A. Hedes,[64] F. Hemmer,[50] C. Henderson,[67] R. Henderson,[14] R. D. L. Henderson,[1] A. M. Hennequin,[50] K. Hennessy,[62] L. Henry,[51] J. Herd,[63] P. Herrero Gascon,[22] J. Heuel,[17] A. Heyn,[13] A. Hicheur,[3] G. Hijano Mendizabal,[52] J. Horswill,[64] R. Hou,[8] Y. Hou,[11] D. C. Houston,[61] N. Howarth,[62] W. Hu,[7] X. Hu,[4] W. Hulsbergen,[38] R. J. Hunter,[58] M. Hushchyn,[44] D. Hutchcroft,[62] M. Idzik,[40] D. Ilin,[44] P. Ilten,[67] A. Iniukhin,[44] A. Iohner,[10] A. Ishteev,[44] K. Ivshin,[44] H. Jage,[17] S. J. Jaimes Elles,[78,49,50] S. Jakobsen,[50] T. Jakoubek,[79] E. Jans,[38] B. K. Jashal,[49] A. Jawahery,[68] C. Jayaweera,[55] A. Jelavic,[1] V. Jevtic,[19] Z. Jia,[16] E. Jiang,[68] X. Jiang,[5,7] Y. Jiang,[7] Y. J. Jiang,[6] E. Jimenez Moya,[9] N. Jindal,[90] M. John,[65] A. John Rubesh Rajan,[23] D. Johnson,[55] C. R. Jones,[57] S. Joshi,[42] B. Jost,[50] J. Juan Castella,[57] N. Jurik,[50] I. Juszczak,[41] K. Kalecinska,[40] D. Kaminaris,[51] S. Kandybei,[53] M. Kane,[60] Y. Kang,[4,l] C. Kar,[11] M. Karacson,[50] A. Kauniskangas,[51] J. W. Kautz,[67] M. K. Kazanecki,[41] F. Keizer,[50] M. Kenzie,[57] T. Ketel,[38] B. Khanji,[70] A. Kharisova,[44] S. Kholodenko,[63,50] G. Khreich,[14] F. Kiraz,[14] T. Kirn,[17] V. S. Kirsebom,[31,c] S. Klaver,[39] N. Kleijne,[35,j] A. Kleimenova,[51] D. K. Klekots,[87] K. Klimaszewski,[42] M. R. Kmiec,[42] T. Knospe,[19] R. Kolb,[22] S. Koliiev,[54] L. Kolk,[19] A. Konoplyannikov,[6] P. Kopciewicz,[50] P. Koppenburg,[38] A. Korchin,[53] I. Kostiuk,[38] O. Kot,[54] S. Kotriakhova,[32] E. Kowalczyk,[68] A. Kozachuk,[44] P. Kravchenko,[44] L. Kravchuk,[44] O. Kravcov,[82] M. Kreps,[58] P. Krokovny,[44] W. Krupa,[70] W. Krzemien,[42] O. Kshyvanskyi,[54] S. Kubis,[85] M. Kucharczyk,[41] V. Kudryavtsev,[44] E. Kulikova,[44] A. Kupsc,[86] V. Kushnir,[53] B. Kutsenko,[13] J. Kvapil,[69] I. Kyryllin,[53] D. Lacarrere,[50] P. Laguarta Gonzalez,[46] A. Lai,[32] A. Lampis,[32] D. Lancierini,[63] C. Landesa Gomez,[48] J. J. Lane,[1] G. Lanfranchi,[28] C. Langenbruch,[22] J. Langer,[19] T. Latham,[58] F. Lazzari,[35,s] C. Lazzeroni,[55] R. Le Gac,[13] H. Lee,[62] R. Lefèvre,[11] A. Leflat,[44] S. Legotin,[44] M. Lehuraux,[58] E. Lemos Cid,[50] O. Leroy,[13] T. Lesiak,[41] E. D. Lesser,[50] B. Leverington,[22] A. Li,[4,l] C. Li,[4] C. Li,[13] H. Li,[74] J. Li,[8] K. Li,[77] L. Li,[64] P. Li,[7] P.-R. Li,[75] Q. Li,[5,7] T. Li,[73] T. Li,[74] Y. Li,[8] Y. Li,[5] Y. Li,[4] Z. Lian,[4,l] Q. Liang,[8] X. Liang,[70] Z. Liang,[32] S. Libralon,[49] A. Lightbody,[12] C. Lin,[7] T. Lin,[59] R. Lindner,[50] H. Linton,[63] R. Litvinov,[32] D. Liu,[8] F. L. Liu,[1] G. Liu,[74] K. Liu,[75] S. Liu,[5] W. Liu,[8] Y. Liu,[60] Y. Liu,[75] Y. L. Liu,[63] G. Loachamin Ordonez,[71] I. Lobo,[1] A. Lobo Salvia,[10] A. Loi,[32] T. Long,[57] F. C. L. Lopes,[2,g] J. H. Lopes,[3] A. Lopez Huertas,[46] C. Lopez Iribarnegaray,[48] S. López Soliño,[48] Q. Lu,[15] C. Lucarelli,[50] D. Lucchesi,[33,u] M. Lucio Martinez,[49] Y. Luo,[6] A. Lupato,[33,v] E. Luppi,[26,f] K. Lynch,[23] S. Lyu,[6] X.-R. Lyu,[7] G. M. Ma,[4,l] H. Ma,[73] S. Maccolini,[19] F. Machefert,[14] F. Maciuc,[43] B. Mack,[70] I. Mackay,[65] L. M. Mackey,[70] L. R. Madhan Mohan,[57] M. J. Madurai,[55] D. Magdalinski,[38] D. Maisuzenko,[44] J. J. Malczewski,[41] S. Malde,[65] L. Malentacca,[50] A. Malinin,[44] T. Maltsev,[44] G. Manca,[32,n] G. Mancinelli,[13] C. Mancuso,[14] R. Manera Escalero,[46] F. M. Manganella,[37] D. Manuzzi,[25] D. Marangotto,[30,k] J. F. Marchand,[10] R. Marchevski,[51] U. Marconi,[25] E. Mariani,[16] S. Mariani,[50] C. Marin Benito,[46] J. Marks,[22] A. M. Marshall,[56] L. Martel,[65] G. Martelli,[34] G. Martellotti,[36] L. Martinazzoli,[50] M. Martinelli,[31,c] D. Martinez Gomez,[83] D. Martinez Santos,[45] F. Martinez Vidal,[49] A. Martorell i Granollers,[47] A. Massafferri,[2] R. Matev,[50] A. Mathad,[50] V. Matiunin,[44] C. Matteuzzi,[70] K. R. Mattioli,[15] A. Mauri,[63] E. Maurice,[15] J. Mauricio,[46] P. Mayencourt,[51] J. Mazorra de Cos,[49] M. Mazurek,[42] D. Mazzanti Tarancon,[46] M. McCann,[63] N. T. McHugh,[61] A. McNab,[64] R. McNulty,[23] B. Meadows,[67] D. Melnychuk,[42] D. Mendoza Granada,[16] P. Menendez Valdes Perez,[48] F. M. Meng,[4,l] M. Merk,[38,84] A. Merli,[51,30] L. Meyer Garcia,[68] D. Miao,[5,7] H. Miao,[7] M. Mikhasenko,[80] D. A. Milanes,[78,w] A. Minotti,[31,c] E. Minucci,[28] T. Miralles,[11] B. Mitreska,[64] D. S. Mitzel,[19] R. Mocanu,[43] A. Modak,[59] L. Moeser,[19] R. D. Moise,[17] E. F. Molina Cardenas,[88] T. Mombächer,[67] M. Monk,[57] T. Monnard,[51] S. Monteil,[11] A. Morcillo Gomez,[48] G. Morello,[28] M. J. Morello,[35,j] M. P. Morgenthaler,[22] A. Moro,[31,c] J. Moron,[40] W. Morren,[38] A. B. Morris,[82,50] A. G. Morris,[13] R. Mountain,[70] Z. Mu,[6] E. Muhammad,[58] F. Muheim,[60] M. Mulder,[38] K. Müller,[52] F. Muñoz-Rojas,[9] V. Mytrochenko,[53] P. Naik,[62] T. Nakada,[51] R. Nandakumar,[59] G. Napoletano,[51] I. Nasteva,[3] M. Needham,[60] E. Nekrasova,[44] N. Neri,[30,k] S. Neubert,[18] N. Neufeld,[50] P. Neustroev,[44] J. Nicolini,[50] D. Nicotra,[84] E. M. Niel,[15] N. Nikitin,[44] L. Nisi,[19] Q. Niu,[75] B. K. Njoki,[50] P. Nogarolli,[3] P. Nogga,[18] C. Normand,[48] J. Novoa Fernandez,[48] G. Nowak,[67] C. Nunez,[88] H. N. Nur,[61] A. Oblakowska-Mucha,[40] V. Obraztsov,[44] T. Oeser,[17] A. Okhotnikov,[44] O. Okhrimenko,[54] R. Oldeman,[32,n] F. Oliva,[60,50] E. Olivart Pino,[46] M. Olocco,[19] R. H. O'Neil,[50] J. S. Ordonez Soto,[11] D. Osthues,[19]

J. M. Otalora Goicochea,[3] P. Owen,[52] A. Oyanguren,[49] O. Ozcelik,[50] F. Paciolla,[35,x] A. Padee,[42] K. O. Padeken,[18] B. Pagare,[48] T. Pajero,[50] A. Palano,[24] L. Palini,[30] M. Palutan,[28] C. Pan,[76] X. Pan,[4,l] S. Panebianco,[12] S. Paniskaki,[50,33] G. Panshin,[5] L. Paolucci,[64] A. Papanestis,[59] M. Pappagallo,[24,p] L. L. Pappalardo,[26] C. Pappenheimer,[67] C. Parkes,[64] D. Parmar,[80] G. Passaleva,[27] D. Passaro,[35,j] A. Pastore,[24] M. Patel,[63] J. Patoc,[65] C. Patrignani,[25,h] A. Paul,[70] C. J. Pawley,[84] A. Pellegrino,[38] J. Peng,[5,7] X. Peng,[75] M. Pepe Altarelli,[28] S. Perazzini,[25] D. Pereima,[44] H. Pereira Da Costa,[69] M. Pereira Martinez,[48] A. Pereiro Castro,[48] C. Perez,[47] P. Perret,[11] A. Perrevoort,[83] A. Perro,[50] M. J. Peters,[67] K. Petridis,[56] A. Petrolini,[29,i] S. Pezzulo,[29,i] J. P. Pfaller,[67] H. Pham,[70] L. Pica,[35,j] M. Piccini,[34] L. Piccolo,[32] B. Pietrzyk,[10] G. Pietrzyk,[14] R. N. Pilato,[62] D. Pinci,[36] F. Pisani,[50] M. Pizzichemi,[31,50,c] V. M. Placinta,[43] M. Plo Casasus,[48] T. Poeschl,[50] F. Polci,[16] M. Poli Lener,[28] A. Poluektov,[13] N. Polukhina,[44] I. Polyakov,[64] E. Polycarpo,[3] S. Ponce,[50] D. Popov,[7,50] K. Popp,[19] S. Poslavskii,[44] K. Prasanth,[60] C. Prouve,[45] D. Provenzano,[32,50,n] V. Pugatch,[54] A. Puicercus Gomez,[50] G. Punzi,[35,s] J. R. Pybus,[69] Q. Qian,[6] W. Qian,[7] N. Qin,[4,l] R. Quagliani,[50] R. I. Rabadan Trejo,[58] R. Racz,[82] J. H. Rademacker,[56] M. Rama,[35] M. Ramírez García,[88] V. Ramos De Oliveira,[71] M. Ramos Pernas,[58] M. S. Rangel,[3] F. Ratnikov,[44] G. Raven,[39] M. Rebollo De Miguel,[49] F. Redi,[30,v] J. Reich,[56] F. Reiss,[20] Z. Ren,[7] P. K. Resmi,[65] M. Ribalda Galvez,[46] R. Ribatti,[51] G. Ricart,[12] D. Riccardi,[35,j] S. Ricciardi,[59] K. Richardson,[66] M. Richardson-Slipper,[57] F. Riehn,[19] K. Rinnert,[62] P. Robbe,[14,50] G. Robertson,[61] E. Rodrigues,[62] A. Rodriguez Alvarez,[46] E. Rodriguez Fernandez,[48] J. A. Rodriguez Lopez,[78] E. Rodriguez Rodriguez,[50] J. Roensch,[19] A. Rogachev,[44] A. Rogovskiy,[59] D. L. Rolf,[19] P. Roloff,[50] V. Romanovskiy,[67] A. Romero Vidal,[48] G. Romolini,[26,50] F. Ronchetti,[51] T. Rong,[6] M. Rotondo,[28] M. S. Rudolph,[70] M. Ruiz Diaz,[22] R. A. Ruiz Fernandez,[48] J. Ruiz Vidal,[84] J. J. Saavedra-Arias,[9] J. J. Saborido Silva,[48] S. E. R. Sacha Emile R.,[50] N. Sagidova,[44] D. Sahoo,[81] N. Sahoo,[55] B. Saitta,[32] M. Salomoni,[31,50,c] I. Sanderswood,[49] R. Santacesaria,[36] C. Santamarina Rios,[48] M. Santimaria,[28] L. Santoro,[2] E. Santovetti,[37] A. Saputi,[26,50] D. Saranin,[44] A. Sarnatskiy,[83] G. Sarpis,[50] M. Sarpis,[82] C. Satriano,[36] A. Satta,[37] M. Saur,[75] D. Savrina,[44] H. Sazak,[17] F. Sborzacchi,[50,28] A. Scarabotto,[19] S. Schael,[17] S. Scherl,[62] M. Schiller,[22] H. Schindler,[50] M. Schmelling,[21] B. Schmidt,[50] N. Schmidt,[69] S. Schmitt,[66] H. Schmitz,[18] O. Schneider,[51] A. Schopper,[63] N. Schulte,[19] M. H. Schune,[14] G. Schwering,[17] B. Sciascia,[28] A. Sciuccati,[50] G. Scriven,[84] I. Segal,[80] S. Sellam,[48] A. Semennikov,[44] T. Senger,[52] M. Senghi Soares,[39] A. Sergi,[29,i] N. Serra,[52] L. Sestini,[27] B. Sevilla Sanjuan,[47] Y. Shang,[6] D. M. Shangase,[88] M. Shapkin,[44] R. S. Sharma,[70] I. Shchemerov,[44] L. Shchutska,[51] T. Shears,[62] L. Shekhtman,[44] J. Shen,[6] Z. Shen,[38] S. Sheng,[51] V. Shevchenko,[44] B. Shi,[7] J. Shi,[57] Q. Shi,[7] W. S. Shi,[74] Y. Shimizu,[14] E. Shmanin,[25] R. Shorkin,[44] R. Silva Coutinho,[2] G. Simi,[33,u] S. Simone,[24,p] M. Singha,[81] I. Siral,[51] N. Skidmore,[58] T. Skwarnicki,[70] M. W. Slater,[55] E. Smith,[66] M. Smith,[63] L. Soares Lavra,[60] M. D. Sokoloff,[67] F. J. P. Soler,[61] A. Solomin,[56] A. Solovev,[44] K. Solovieva,[20] N. S. Sommerfeld,[18] R. Song,[1] Y. Song,[51] Y. Song,[4,l] Y. S. Song,[6] F. L. Souza De Almeida,[46] B. Souza De Paula,[3] K. M. Sowa,[40] E. Spadaro Norella,[29,i] E. Spedicato,[25] J. G. Speer,[19] P. Spradlin,[61] F. Stagni,[50] M. Stahl,[80] S. Stahl,[50] S. Stanislaus,[65] M. Stefaniak,[90] O. Steinkamp,[52] D. Strekalina,[44] Y. Su,[7] F. Suljik,[65] J. Sun,[32] J. Sun,[64] L. Sun,[76] D. Sundfeld,[2] W. Sutcliffe,[52] P. Svihra,[79] V. Svintozelskyi,[49] K. Swientek,[40] F. Swystun,[57] A. Szabelski,[42] T. Szumlak,[40] Y. Tan,[4] Y. Tang,[76] Y. T. Tang,[7] M. D. Tat,[22] J. A. Teijeiro Jimenez,[48] A. Terentev,[44] F. Terzuoli,[35,x] F. Teubert,[50] E. Thomas,[50] D. J. D. Thompson,[55] A. R. Thomson-Strong,[60] H. Tilquin,[63] V. Tisserand,[11] S. T'Jampens,[10] M. Tobin,[5,50] T. T. Todorov,[20] L. Tomassetti,[26,f] G. Tonani,[30] X. Tong,[6] T. Tork,[30] L. Toscano,[19] D. Y. Tou,[4,l] C. Trippl,[47] G. Tuci,[22] N. Tuning,[38] L. H. Uecker,[22] A. Ukleja,[40] D. J. Unverzagt,[22] A. Upadhyay,[50] B. Urbach,[60] A. Usachov,[38] A. Ustyuzhanin,[44] U. Uwer,[22] V. Vagnoni,[25,50] A. Vaitkevicius,[82] V. Valcarce Cadenas,[48] G. Valenti,[25] N. Valls Canudas,[50] J. van Eldik,[50] H. Van Hecke,[69] E. van Herwijnen,[63] C. B. Van Hulse,[48,y] R. Van Laak,[51] M. van Veghel,[84] G. Vasquez,[52] R. Vazquez Gomez,[46] P. Vazquez Regueiro,[48] C. Vázquez Sierra,[45] S. Vecchi,[26] J. Velilla Serna,[49] J. J. Velthuis,[56] M. Veltri,[27,z] A. Venkateswaran,[51] M. Verdoglia,[32] M. Vesterinen,[58] W. Vetens,[70] D. Vico Benet,[65] P. Vidrier Villalba,[46] M. Vieites Diaz,[48] X. Vilasis-Cardona,[47] E. Vilella Figueras,[62] A. Villa,[25] P. Vincent,[16] B. Vivacqua,[3] F. C. Volle,[55] D. vom Bruch,[13] N. Voropaev,[44] K. Vos,[84] C. Vrahas,[60] J. Wagner,[19] J. Walsh,[35] E. J. Walton,[1] G. Wan,[6] A. Wang,[7] B. Wang,[5] C. Wang,[22] G. Wang,[8] H. Wang,[75] J. Wang,[7] J. Wang,[5] J. Wang,[4,l] J. Wang,[76] M. Wang,[50] N. W. Wang,[7] R. Wang,[56]

X. Wang,[8] X. Wang,[74] X. W. Wang,[63] Y. Wang,[77] Y. Wang,[6] Y. H. Wang,[75] Z. Wang,[14] Z. Wang,[30] J. A. Ward,[58,1] M. Waterlaat,[50] N. K. Watson,[55] D. Websdale,[63] Y. Wei,[6] Z. Weida,[7] J. Wendel,[45] B. D. C. Westhenry,[56] C. White,[57] M. Whitehead,[61] E. Whiter,[55] A. R. Wiederhold,[64] D. Wiedner,[19] M. A. Wiegertjes,[38] C. Wild,[65] G. Wilkinson,[65,50] M. K. Wilkinson,[67] M. Williams,[66] M. J. Williams,[50] M. R. J. Williams,[60] R. Williams,[57] S. Williams,[56] Z. Williams,[56] F. F. Wilson,[59] M. Winn,[12] W. Wislicki,[42] M. Witek,[41] L. Witola,[19] T. Wolf,[22] E. Wood,[57] G. Wormser,[14] S. A. Wotton,[57] H. Wu,[70] J. Wu,[8] X. Wu,[76] Y. Wu,[6,57] Z. Wu,[7] K. Wyllie,[50] S. Xian,[74] Z. Xiang,[5] Y. Xie,[8] T. X. Xing,[30] A. Xu,[35,j] L. Xu,[4,l] M. Xu,[50] Z. Xu,[50] Z. Xu,[7] Z. Xu,[5] S. Yadav,[26] K. Yang,[63] X. Yang,[6] Y. Yang,[81] Y. Yang,[7] Z. Yang,[6] H. Yeung,[64] H. Yin,[8] X. Yin,[7] C. Y. Yu,[6] J. Yu,[73] X. Yuan,[5] Y Yuan,[5,7] J. A. Zamora Saa,[72] M. Zavertyaev,[21] M. Zdybal,[41] F. Zenesini,[25] C. Zeng,[5,7] M. Zeng,[4,l] C. Zhang,[6] D. Zhang,[8] J. Zhang,[7] L. Zhang,[4,l] R. Zhang,[8] S. Zhang,[65] S. L. Zhang,[73] Y. Zhang,[6] Y. Z. Zhang,[4,l] Z. Zhang,[4,l] Y. Zhao,[22] A. Zhelezov,[22] S. Z. Zheng,[6] X. Z. Zheng,[4,l] Y. Zheng,[7] T. Zhou,[6] X. Zhou,[8] V. Zhovkovska,[58] L. Z. Zhu,[7] X. Zhu,[4,l] X. Zhu,[8] Y. Zhu,[17] V. Zhukov,[17] J. Zhuo,[49] D. Zuliani,[33,u] and G. Zunica[28]

(LHCb Collaboration)

[1]*School of Physics and Astronomy, Monash University, Melbourne, Australia*
[2]*Centro Brasileiro de Pesquisas Físicas (CBPF), Rio de Janeiro, Brazil*
[3]*Universidade Federal do Rio de Janeiro (UFRJ), Rio de Janeiro, Brazil*
[4]*Department of Engineering Physics, Tsinghua University, Beijing, China*
[5]*Institute Of High Energy Physics (IHEP), Beijing, China*
[6]*School of Physics State Key Laboratory of Nuclear Physics and Technology, Peking University, Beijing, China*
[7]*University of Chinese Academy of Sciences, Beijing, China*
[8]*Institute of Particle Physics, Central China Normal University, Wuhan, Hubei, China*
[9]*Consejo Nacional de Rectores (CONARE), San Jose, Costa Rica*
[10]*Université Savoie Mont Blanc, CNRS, IN2P3-LAPP, Annecy, France*
[11]*Université Clermont Auvergne, CNRS/IN2P3, LPC, Clermont-Ferrand, France*
[12]*Université Paris-Saclay, Centre d'Etudes de Saclay (CEA), IRFU, Gif-Sur-Yvette, France*
[13]*Aix Marseille Univ, CNRS/IN2P3, CPPM, Marseille, France*
[14]*Université Paris-Saclay, CNRS/IN2P3, IJCLab, Orsay, France*
[15]*Laboratoire Leprince-Ringuet, CNRS/IN2P3, Ecole Polytechnique, Institut Polytechnique de Paris, Palaiseau, France*
[16]*Laboratoire de Physique Nucléaire et de Hautes Énergies (LPNHE), Sorbonne Université, CNRS/IN2P3, Paris, France*
[17]*I. Physikalisches Institut, RWTH Aachen University, Aachen, Germany*
[18]*Universität Bonn - Helmholtz-Institut für Strahlen und Kernphysik, Bonn, Germany*
[19]*Fakultät Physik, Technische Universität Dortmund, Dortmund, Germany*
[20]*Physikalisches Institut, Albert-Ludwigs-Universität Freiburg, Freiburg, Germany*
[21]*Max-Planck-Institut für Kernphysik (MPIK), Heidelberg, Germany*
[22]*Physikalisches Institut, Ruprecht-Karls-Universität Heidelberg, Heidelberg, Germany*
[23]*School of Physics, University College Dublin, Dublin, Ireland*
[24]*INFN Sezione di Bari, Bari, Italy*
[25]*INFN Sezione di Bologna, Bologna, Italy*
[26]*INFN Sezione di Ferrara, Ferrara, Italy*
[27]*INFN Sezione di Firenze, Firenze, Italy*
[28]*INFN Laboratori Nazionali di Frascati, Frascati, Italy*
[29]*INFN Sezione di Genova, Genova, Italy*
[30]*INFN Sezione di Milano, Milano, Italy*
[31]*INFN Sezione di Milano-Bicocca, Milano, Italy*
[32]*INFN Sezione di Cagliari, Monserrato, Italy*
[33]*INFN Sezione di Padova, Padova, Italy*
[34]*INFN Sezione di Perugia, Perugia, Italy*
[35]*INFN Sezione di Pisa, Pisa, Italy*
[36]*INFN Sezione di Roma La Sapienza, Roma, Italy*
[37]*INFN Sezione di Roma Tor Vergata, Roma, Italy*
[38]*Nikhef National Institute for Subatomic Physics, Amsterdam, Netherlands*
[39]*Nikhef National Institute for Subatomic Physics and VU University Amsterdam, Amsterdam, Netherlands*
[40]*AGH - University of Krakow, Faculty of Physics and Applied Computer Science, Kraków, Poland*

[41]Henryk Niewodniczanski Institute of Nuclear Physics Polish Academy of Sciences, Kraków, Poland
[42]National Center for Nuclear Research (NCBJ), Warsaw, Poland
[43]Horia Hulubei National Institute of Physics and Nuclear Engineering, Bucharest-Magurele, Romania
[44]Authors affiliated with an institute formerly covered by a cooperation agreement with CERN
[45]Universidade da Coruña, A Coruña, Spain
[46]ICCUB, Universitat de Barcelona, Barcelona, Spain
[47]La Salle, Universitat Ramon Llull, Barcelona, Spain
[48]Instituto Galego de Física de Altas Enerxías (IGFAE), Universidade de Santiago de Compostela, Santiago de Compostela, Spain
[49]Instituto de Fisica Corpuscular, Centro Mixto Universidad de Valencia - CSIC, Valencia, Spain
[50]European Organization for Nuclear Research (CERN), Geneva, Switzerland
[51]Institute of Physics, Ecole Polytechnique Fédérale de Lausanne (EPFL), Lausanne, Switzerland
[52]Physik-Institut, Universität Zürich, Zürich, Switzerland
[53]NSC Kharkiv Institute of Physics and Technology (NSC KIPT), Kharkiv, Ukraine
[54]Institute for Nuclear Research of the National Academy of Sciences (KINR), Kyiv, Ukraine
[55]School of Physics and Astronomy, University of Birmingham, Birmingham, United Kingdom
[56]H.H. Wills Physics Laboratory, University of Bristol, Bristol, United Kingdom
[57]Cavendish Laboratory, University of Cambridge, Cambridge, United Kingdom
[58]Department of Physics, University of Warwick, Coventry, United Kingdom
[59]STFC Rutherford Appleton Laboratory, Didcot, United Kingdom
[60]School of Physics and Astronomy, University of Edinburgh, Edinburgh, United Kingdom
[61]School of Physics and Astronomy, University of Glasgow, Glasgow, United Kingdom
[62]Oliver Lodge Laboratory, University of Liverpool, Liverpool, United Kingdom
[63]Imperial College London, London, United Kingdom
[64]Department of Physics and Astronomy, University of Manchester, Manchester, United Kingdom
[65]Department of Physics, University of Oxford, Oxford, United Kingdom
[66]Massachusetts Institute of Technology, Cambridge, Massachusetts, USA
[67]University of Cincinnati, Cincinnati, Ohio, USA
[68]University of Maryland, College Park, Maryland, USA
[69]Los Alamos National Laboratory (LANL), Los Alamos, New Mexico, USA
[70]Syracuse University, Syracuse, New York, USA
[71]Pontifícia Universidade Católica do Rio de Janeiro (PUC-Rio), Rio de Janeiro, Brazil (associated with Universidade Federal do Rio de Janeiro (UFRJ), Rio de Janeiro, Brazil)
[72]Universidad Andres Bello, Santiago, Chile (associated with Physik-Institut, Universität Zürich, Zürich, Switzerland)
[73]School of Physics and Electronics, Hunan University, Changsha City, China (associated with Institute of Particle Physics, Central China Normal University, Wuhan, Hubei, China)
[74]State Key Laboratory of Nuclear Physics and Technology, South China Normal University, Guangzhou, China (associated with Department of Engineering Physics, Tsinghua University, Beijing, China)
[75]Lanzhou University, Lanzhou, China [associated with Institute Of High Energy Physics (IHEP), Beijing, China]
[76]School of Physics and Technology, Wuhan University, Wuhan, China (associated with Department of Engineering Physics, Tsinghua University, Beijing, China)
[77]Henan Normal University, Xinxiang, China (associated with Institute of Particle Physics, Central China Normal University https://ror.org/03x1jna21, Wuhan, Hubei, China)
[78]Departamento de Fisica, Universidad Nacional de Colombia, Bogota, Colombia (associated with Laboratoire de Physique Nucléaire et de Hautes Énergies (LPNHE), Sorbonne Université, CNRS/IN2P3, Paris, France)
[79]Institute of Physics of the Czech Academy of Sciences, Prague, Czech Republic (associated with Department of Physics and Astronomy, University of Manchester, Manchester, United Kingdom)
[80]Ruhr Universitaet Bochum, Fakultaet f. Physik und Astronomie, Bochum, Germany (associated with Fakultät Physik, Technische Universität Dortmund, Dortmund, Germany)
[81]Eotvos Lorand University, Budapest, Hungary (associated with European Organization for Nuclear Research (CERN), Geneva, Switzerland)
[82]Faculty of Physics, Vilnius University, Vilnius, Lithuania (associated with Physikalisches Institut, Albert-Ludwigs-Universität Freiburg, Freiburg, Germany)
[83]Van Swinderen Institute, University of Groningen, Groningen, Netherlands (associated with Nikhef National Institute for Subatomic Physics, Amsterdam, Netherlands)
[84]Universiteit Maastricht, Maastricht, Netherlands (associated with Nikhef National Institute for Subatomic Physics, Amsterdam, Netherlands)
[85]Tadeusz Kosciuszko Cracow University of Technology, Cracow, Poland (associated with Henryk Niewodniczanski Institute of Nuclear Physics Polish Academy of Sciences, Kraków, Poland)
[86]Department of Physics and Astronomy, Uppsala University, Uppsala, Sweden (associated with School of Physics and Astronomy, University of Glasgow, Glasgow, United Kingdom)

[87]*Taras Schevchenko University of Kyiv, Faculty of Physics, Kyiv, Ukraine (associated with Université Paris-Saclay, CNRS/IN2P3, IJCLab, Orsay, France)*
[88]*University of Michigan, Ann Arbor, Michigan, USA (associated with Syracuse University, Syracuse, New York, USA)*
[89]*Indiana University, Bloomington, Indiana, USA [associated with Los Alamos National Laboratory (LANL), Los Alamos, New Mexico, USA]*
[90]*Ohio State University, Columbus, Ohio, USA [associated with Los Alamos National Laboratory (LANL), Los Alamos, New Mexico, USA]*

[a]Deceased.
[b]Also at Lamarr Institute for Machine Learning and Artificial Intelligence, Dortmund, Germany.
[c]Also at Università degli Studi di Milano-Bicocca, Milano, Italy.
[d]Also at Università di Modena e Reggio Emilia, Modena, Italy.
[e]Also at Department of Physics and Astronomy, University of Victoria, Victoria, British Columbia, Canada.
[f]Also at Università di Ferrara, Ferrara, Italy.
[g]Also at Universidade Estadual de Campinas (UNICAMP), Campinas, Brazil.
[h]Also at Università di Bologna, Bologna, Italy.
[i]Also at Università di Genova, Genova, Italy.
[j]Also at Scuola Normale Superiore, Pisa, Italy.
[k]Also at Università degli Studi di Milano, Milano, Italy.
[l]Also at Center for High Energy Physics, Tsinghua University, Beijing, China.
[m]Also at Universidad Nacional Autónoma de Honduras, Tegucigalpa, Honduras.
[n]Also at Università di Cagliari, Cagliari, Italy.
[o]Also at Centro Federal de Educacão Tecnológica Celso Suckow da Fonseca, Rio De Janeiro, Brazil.
[p]Also at Università di Bari, Bari, Italy.
[q]Also at Università di Perugia, Perugia, Italy.
[r]Also at LIP6, Sorbonne Université, Paris, France.
[s]Also at Università di Pisa, Pisa, Italy.
[t]Also at Hangzhou Institute for Advanced Study, UCAS, Hangzhou, China.
[u]Also at Università di Padova, Padova, Italy.
[v]Also at Università di Bergamo, Bergamo, Italy.
[w]Also at Universidad de Ingeniería y Tecnología (UTEC), Lima, Peru.
[x]Also at Università di Siena, Siena, Italy.
[y]Also at Universidad de Alcalá, Alcalá de Henares, Spain.
[z]Also at Università di Urbino, Urbino, Italy.